Soft Matter

PAPER

View Article Online
View Journal | View Issue

Cite this: *Soft Matter*, 2023, **19**, 2654

Self-assembly of dodecagonal and octagonal quasicrystals in hard spheres on a plane†

Etienne Fayen, [a] Marianne Impéror-Clerc, [a] Laura Filion, [b] Giuseppe Foffi [a] and Frank Smallenburg *[a]

Received 12th February 2023,
Accepted 17th March 2023

DOI: 10.1039/d3sm00179b

rsc.li/soft-matter-journal

Hard spheres are one of the most fundamental model systems in soft matter physics, and have been instrumental in shedding light on nearly every aspect of classical condensed matter. Here, we add one more important phase to the list that hard spheres form: quasicrystals. Specifically, we use simulations to show that an extremely simple, purely entropic model system, consisting of two sizes of hard spheres resting on a flat plane, can spontaneously self-assemble into two distinct random-tiling quasicrystal phases. The first quasicrystal is a dodecagonal square-triangle tiling, commonly observed in a large variety of colloidal systems. The second quasicrystal has, to our knowledge, never been observed in either experiments or simulations. It exhibits octagonal symmetry, and consists of three types of tiles: triangles, small squares, and large squares, whose relative concentration can be continuously varied by tuning the number of smaller spheres present in the system. The observed tile composition of the self-assembled quasicrystals agrees very well with the theoretical prediction we obtain by considering the four-dimensional (lifted) representation of the quasicrystal. Both quasicrystal phases form reliably and rapidly over a significant part of parameter space. Our results demonstrate that entropy combined with a set of geometrically compatible, densely packed tiles can be sufficient ingredients for the self-assembly of colloidal quasicrystals.

1 Introduction

Hard spheres are arguably the most fundamental model system in colloid science. The colloidal equivalent of marbles, hard spheres only interact when colliding, but despite this simplicity exhibit nearly all important aspects of phase behavior. As such, colloidal hard spheres have been instrumental in enhancing our understanding of crystal nucleation,[1,2] crystallization in confinement,[3–9] two-dimensional melting,[10,11] glassy dynamics,[12–16] crystal defects,[17–19] among many others. Their important role in soft matter science stems from their theoretical simplicity, which makes them a natural first approximation for particles with a hard core, as well as the fact that they can be quantitatively reproduced in the lab.[20–23] One aspect of colloidal phase behavior where hard spheres have thus far not proven suitable as a model system is the formation of quasicrystals. These exotic structures possess long-range order but lack periodicity and typically exhibit so-called "forbidden" symmetries, incompatible with periodic crystalline order. They have been predicted to form or directly observed in a variety of soft-matter systems consisting of nanoparticles or macromolecules,[24–27] as well as in several (non-additive) 2D binary Lennard-Jones mixtures,[28–31] but have so far remained elusive in colloidal particles on the micrometer scale.

This is unfortunate, as such a colloidal model system that reliably forms quasicrystals would be ideal for the real-time study of quasicrystal self-assembly. In computer simulations of colloidal soft matter, quasicrystals are typically found in systems with highly specific interactions – such as oscillatory potentials, patchy interactions, and square-shoulder repulsion[24,32–37] – which are hard to realize in the lab. While complex quasicrystal approximants have been found to self-assemble in simulations of polydisperse mixtures of hard spheres,[38] and finite clusters with icosahedral symmetry have been shown to form in spherical confinement,[3,4,39] to date hard-sphere systems have not been found to be capable of forming a quasicrystal.

Here, we demonstrate quasicrystal self-assembly in binary mixtures of hard spheres lying on a flat plane. In particular, we find that this simple, purely entropic quasi-two-dimensional system exhibits an amazingly rich self-assembly behavior, forming not only six periodic crystal phases, but two random-tiling quasicrystals as well: one dodecagonal and one octagonal. Although dodecagonal quasicrystals are relatively common in soft matter models,[25,32,33,40–42] octagonal ones are much

[a] *Université Paris-Saclay, CNRS, Laboratoire de Physique des Solides, 91405, Orsay, France. E-mail: frank.smallenburg@cnrs.fr*
[b] *Soft Condensed Matter, Debye Institute for Nanomaterials Science, Utrecht University, Utrecht, The Netherlands*

† Electronic supplementary information (ESI) available. See DOI: https://doi.org/10.1039/d3sm00179b

more rare.[33–36] Moreover, unlike previously observed eight-fold quasicrystals made up of two tiles, the octagonal tiling we observe here is composed of three distinct tiles, whose relative composition can be directly tuned by changing the fraction of small spheres in the system. Both quasicrystal phases form reliably and rapidly over a significant part of parameter space. As binary hard spheres on a plane are directly experimentally realizable, to the point where they quantitatively match simulations,[10,43] this discovery identifies an ideal model system for studying essentially all properties of quasicrystals, including their structure, nucleation, melting, and defect dynamics.

2 Model

We consider mixtures of hard spheres of two different sizes constrained to lie on a flat plane. As illustrated in Fig. 1, this system can be mapped onto an equivalent 2D one by looking at its projection on the substrate, where spheres become disks. As the particles are constrained to move in only two dimensions, the disks corresponding to spheres of equal size cannot overlap, and hence interact simply as hard disks. However, for spheres of different sizes, a small amount of overlap of the 2D projections of the particles is allowed. Specifically, the distance of closest approach between the projections of a large particle of diameter σ_L and a small particle of diameter σ_S is given by the geometric mean of their diameters $\sigma_{LS} = \sqrt{\sigma_L \sigma_S}$.

The phase behavior of a mixture of N_L large spheres and N_S small spheres confined to a substrate with area A is controlled by three parameters: the size ratio $q = \sigma_S/\sigma_L$, the fraction of small spheres $x_S = N_S/(N_L + N_S)$, and the packing fraction $\eta = (N_S\sigma_S^2 + N_L\sigma_L^2)\pi/4A$ occupied by the equivalent 2D disks. Note that since some overlap is allowed between different species in the 2D projection, the total packing fraction may exceed 1 in some cases.

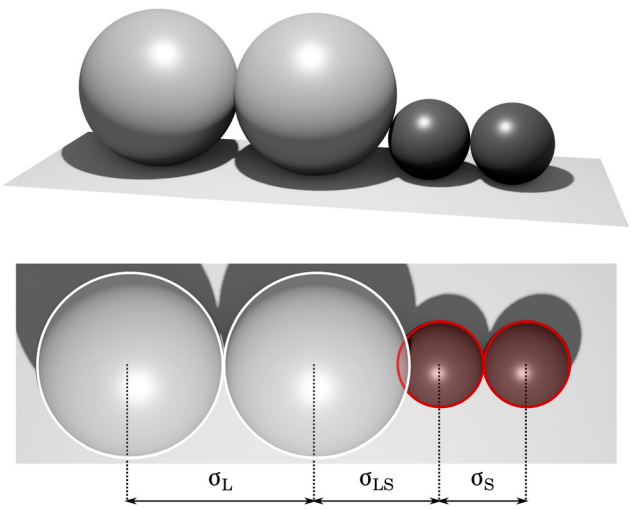

Fig. 1 Schematic depiction of the model. 3D hard spheres lying on a flat surface (top) can be interpreted as an equivalent 2D system of non-additive hard disks (bottom). Spheres of the same type behave like standard hard disks (their projections cannot overlap), while the closest projected distance between particles of different types σ_{LS} is smaller than the sum of the radii.

3 Infinite pressure phase behavior

Even for simple binary mixtures in 2D, the number of different ordered structures that can emerge can be quite large and difficult to enumerate. To obtain an impression of the crystals we might expect to find, we used a technique specifically designed to detect the close-packing crystal structures that would form in the limit of infinite pressure. To this end, we followed ref. 44 to map out the infinite pressure phase diagram of non-additive hard disks. Specifically, for a range of size ratios and compositions, we construct a library of candidate crystal structures and find – for each combination of q and x_S – the best-packed phase or coexistence of phases. Note that in the notation of ref. 44, the present case of spheres lying on a flat plane corresponds to a size-ratio-dependent non-additivity parameter

$$\Delta(q) = 2\sqrt{q}/(1+q) - 1, \quad (1)$$

such that the contact distance between a small and a large sphere can be written as

$$\sigma_{LS} = (1+\Delta)\frac{\sigma_L + \sigma_S}{2}. \quad (2)$$

For each size ratio, we use the data from ref. 44 for the best packed candidate structures, which were obtained from systematic sampling of unit cells containing up to 12 particles using Monte Carlo simulations with a variable box shape.[46] The infinite pressure phase diagram is then constructed from these structures by common-tangent construction,[44] and shown in Fig. 2.

In addition to the trivial monodisperse hexagonal crystal phases of the large or small particles (Hex_L and Hex_S, respectively), we observe a wide variety of binary phases. Since any pure crystal phase can only occur at a single composition x_S, the densest-packed state at most points in the phase diagram (white regions) is a coexistence between two crystal phases at different compositions: the ones appearing directly above and below the chosen state point. In addition to the expected monodisperse hexagonal crystals of either large or small particles, we find a variety of binary crystal phases, many of which are similar to those found in additive systems.[44,45] Note that for large size ratios, the system becomes almost additive. In the additive case, it is proven that there exist no denser structures than a coexistence of Hex_L and Hex_S for $q \gtrsim 0.74$.[47] Therefore we expect no additional binary crystal phases to appear at size ratios above our investigated range $0.3 \leq q \leq 0.75$.

For each phase in Fig. 2 we also depict the repeating unit that can be used to construct the crystal phase, which we call a tile. Unlike a unit cell, tiles can appear in the full crystal structure in multiple orientations. Interestingly, for certain coexistence regions, the two coexisting phases consist of tiles that can mix. One realization of this occurs at low size ratios ($q \simeq 0.3$) where the T1 and Hex_L phases consist of identical

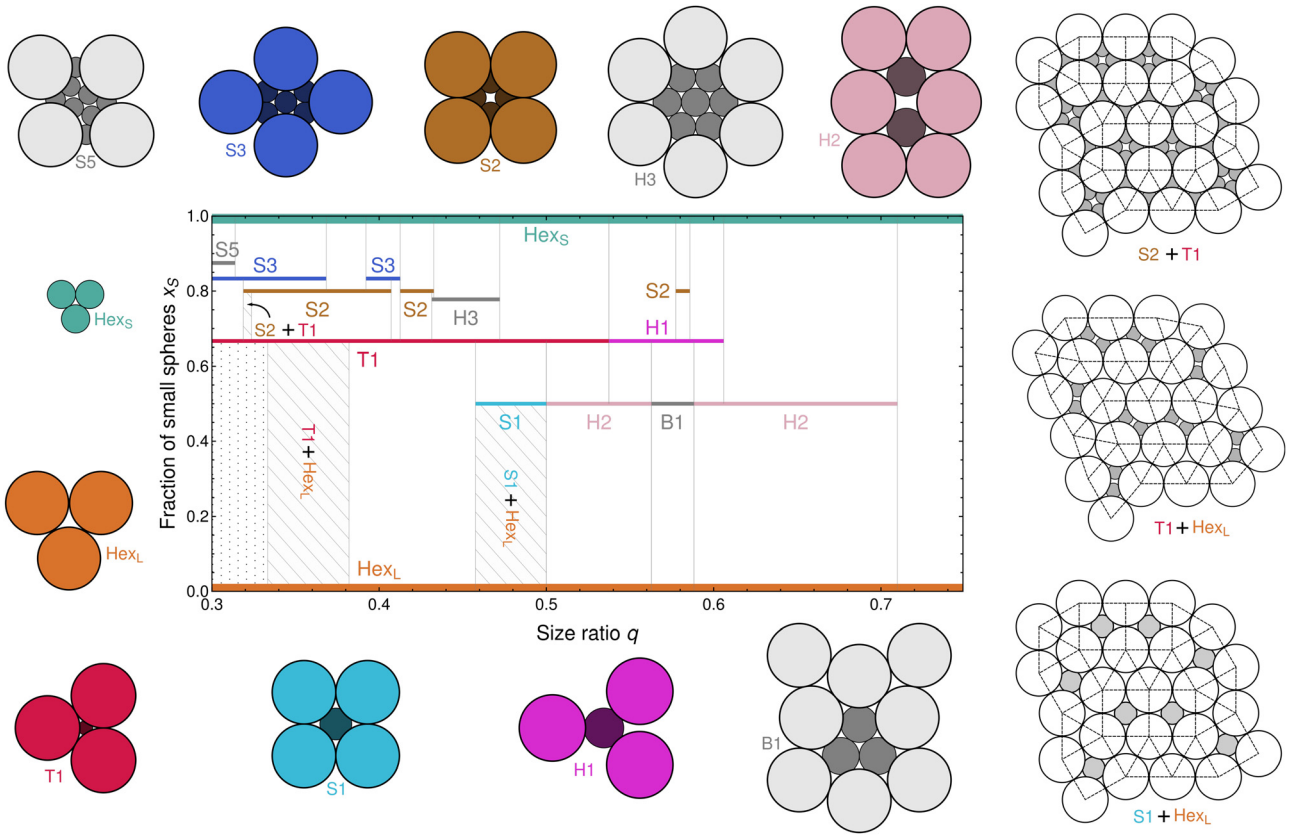

Fig. 2 Infinite-pressure phase behavior of binary mixtures of spheres on a flat plane, as a function of the size ratio q and fraction of small particles x_S. Phases are labeled following the naming scheme of ref. 44, 45. The white regions correspond to coexistence regions between the phases directly above and below. The striped and dotted areas indicate regions where these two phases can form random tilings or a lattice gas, respectively. Examples of finite patches of the three possible random tilings, corresponding to the striped regions in the diagram, are displayed on the right.

triangles of large particles, but decorated differently by small particles. In the region where these two phases mix, they can form a lattice gas where tiles of T1 and Hex_L are randomly mixed (dotted region in Fig. 2). Another, much more interesting situation occurs when two tiles of different shapes can mix. This occurs in the three striped regions in Fig. 2. For example, at size ratios just below $q = 0.5$, the square tile of the S1 phase has the same edge length as the triangular tile of the Hex_L phase, allowing them to mix and form a space-filling square-triangle tiling,[44,45] illustrated in the bottom right of Fig. 2. As this mixing increases the entropy without lowering the packing fraction, the expected phase at infinite pressure here is a random tiling of squares and triangles, which at an ideal composition $x_S = (3 - \sqrt{3})/4 \simeq 0.317$ is known to have 12-fold symmetry on average.[48,49] Two closely related tilings, also illustrated in Fig. 2 are found at lower size ratios. As a result, one intriguing prediction from Fig. 2 is the possibility of a 12-fold quasicrystal self-assembling from simple binary mixtures of colloidal spheres on a substrate.

4 Finite pressure self-assembly

In practice, the infinite-pressure phase behavior is not a reliable indication for the phases one might find in a real self-assembly experiment. Self-assembly in a colloidal system takes place at finite pressure, where particles can diffuse to reach their lattice site and vibrate around it. This brings vibrational entropy contributions to the free energy of different crystal phases which can fundamentally change the phase behavior. Moreover, dynamical arrest or competition with other candidate phases can prevent the reliable formation of a crystal even if it is thermodynamically stable.

Hence, for a more realistic look at the self-assembly, we perform computer simulations at finite pressure for an extensive grid of state points spanning size ratios $0.25 \leq q \leq 0.75$, compositions $0.05 \leq x_S \leq 0.95$, and packing fractions $0.7 \leq \eta \leq 1.0$. In particular, we run event-driven molecular dynamics (EDMD) simulations[50] in the canonical ensemble, *i.e.* at constant number of particles N, volume V, and temperature T. The simulation algorithm is an adaptation of the methods described in ref. 51. We perform the EDMD simulations in the microcanonical ensemble, *i.e.* at constant number of particles N, volume V, and energy E. Initial configurations are obtained by starting in a dilute state at the desired composition, and then performing an EDMD simulation in which the particle diameters grow until the desired packing fraction is reached.

We perform a systematic exploration of parameter space for systems of $N = 2000$ particles, varying the composition x_S

between 0.05 and 0.95 in steps of 0.05 and the size ratio q between 0.25 and 0.75 in steps of 0.05. The packing fraction η ranged from 0.7 to up to 1.0 in steps of 0.01, where we only considered state points where the growing-particle simulations were able to rapidly reach the desired packing fraction without jamming. In other words, we assume that at packing fractions where jamming occurs during our initial compression, the system would likely be too densely packed to observe self-assembly on a reasonable time scale. Each self-assembly simulation is allowed to run for at least $10^6\tau_{MD}$, with $\tau_{MD} = \sqrt{m\sigma_L^2/k_BT}$ the simulation time unit, m the mass of a particle (chosen equal for both species), σ_L the large-particle diameter, and k_B Boltzmann's constant. Subsequently, longer simulations were performed for state points where self-assembly was considered likely to occur on a reasonable time-scale based on the final pressure of the first simulations. In particular, we extended the simulations at state points with a pressure $16 \lessapprox P\sigma_L^2/k_BT \lessapprox 33$ to a total length of $5 \times 10^6\tau_{MD}$.

Our results are summarized in Fig. 3. The central diagram reports for each investigated combination of q and x_S what ordered phases were observed. We consider a crystal to have self-assembled for a given combination of q and x_S when we find significant clusters of the crystal in the simulation box for at least one packing fraction. Our simulations show that a number of the best-packed phases we predicted in Fig. 2 indeed spontaneously self-assemble. Naturally, this includes the trivial

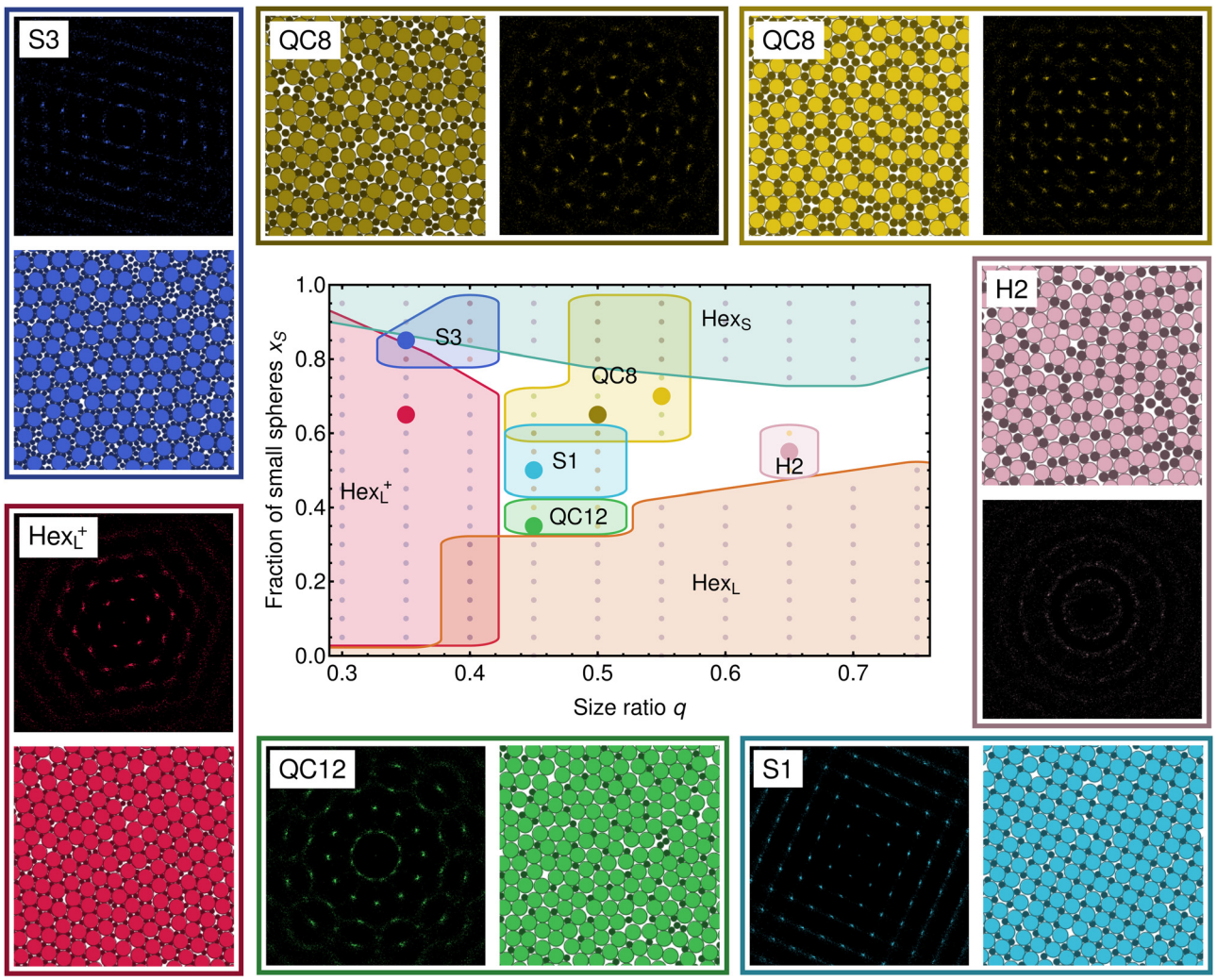

Fig. 3 Self-assembly diagram for binary mixtures of spheres on a flat plane, as a function of the size ratio q and fraction of small particles x_S. For each combination of q and x_S, we perform simulations at a range of different packing fractions, and report the observed phases. Points in the phase diagram contained in a colored region display the self-assembly of the corresponding phase. For each binary crystal phase, we include a representative snapshot (marked as a large dot of the corresponding phase color) and the scattering pattern that results from a Fourier transform of the positions of the large spheres. For the QC8 phase, we include two snapshots: one containing a large concentration of S1 squares (top middle) and one containing a large concentration of S2 squares (top right). Hex$_L$ and Hex$_S$ are hexagonal crystals consisting of only large or small spheres, respectively, and are not depicted. Note that at some state points, we find the self-assembly of two different phases that are either in coexistence or occur at different packing fractions – hence some of the crystal regions overlap. At state points without an indicated crystal phase, no crystallization was observed at any of the investigated packing fractions.

hexagonal crystals of the large and small spheres (Hex_L and Hex_S) that can be found at compositions close to $x_S = 0$ and 1, respectively. Additionally, we observe large-scale crystallization into the S1 and S3 phases close to the regions expected from Fig. 2. We also observe the more complex H2 phase, albeit only in finite clusters – a closer inspection of the systems where these form show a very low overall mobility of the system, suggesting that crystallization of this phase is hindered by slow dynamics. For sufficiently low q, the system nearly always forms a hexagonal lattice of large spheres, with the small spheres interspersed between them (labeled Hex_S^+). Depending on the composition, this may look similar to the T1 phase (as depicted in the sample snapshot in Fig. 3), but the number of small spheres per triangular cavity in the lattice of large spheres appears to continuously depend on the composition x_S (see ESI†). For $x_S < 2/3$, this simply means that a random selection of the triangular holes are empty, resulting in a lattice gas or interstitial solid solution.[44,45] For larger x_S, progressively more small particles are included between the large spheres, but we observe no clear structural transition between these regimes. Hence, we choose to collectively indicate this region as Hex_S^+.

Most intriguingly, in addition to these periodic phases, we also observe the self-assembly of two distinct quasicrystals, both at size ratios between $q = 0.45$ and $q = 0.55$. The dodecagonal quasicrystal (QC12) that appears at low fractions of small spheres is indeed the square-triangle tiling[48,49] expected from the infinite-pressure diagram. It is made of regular squares and triangles (S1 and Hex_L tiles). This quasicrystal is analogous to a number of quasicrystals observed in soft matter systems, including patchy particles with five attractive patches,[32] hard disks with a square-shoulder repulsion,[40,41] binary mixtures of nanoparticles,[25] block copolymers,[26,27] and soft repulsive colloids.[33] Additionally, various 3D systems have been shown to form quasicrystals consisting of layers of a square-triangle tiling.[42,52,53] The second quasicrystal (QC8) has octagonal symmetry, and consists of a mixture of three tiles: the isosceles triangles that appear in the H1 phase, the squares from the S1 lattice, and the larger squares from the S2 lattice.

For the quasicrystals, local crystalline order is typically hard to see by eye, and we instead rely on the symmetry of the scattering pattern for our classification. In particular, for each simulation, we measured the two-dimensional structure factor of the final configuration using

$$S(\mathbf{k}) = \frac{1}{N}\left|\sum_{n=1}^{N}\exp(i\mathbf{k}\cdot\mathbf{r}_n)\right|^2. \quad (3)$$

where k is a wave vector commensurate with the periodic simulation box, and r_n is the position of particle n. We plot the resulting scattering pattern $S(k)$ in two dimensions *via* a logarithmic color scale. The resulting scattering patterns for selected state points are included in Fig. 3. Note that in the ESI† Data, we include a full catalogue of all final configurations and their diffraction patterns.

5 Quasicrystal analysis

In order to examine the QC12 and QC8 quasiperiodic structures in more detail, we perform additional simulations of $N = 10\,000$ particles in the regime where they are found to self-assemble. In the final configurations, we reconstruct the underlying tiling from the bond network (see ESI†) and use it to analyse the quasicrystals.

In Fig. 4, we show portions of the final state of three simulated mixtures of 10^4 particles, at different state points: one corresponding to the QC12 phase and two corresponding to the QC8 phase. Note that the two QC8 snapshots consist primarily of the same three tiles, but mixed in different concentrations. The first is dominated by small squares, while the second, which contains more small particles, predominantly contains large squares. Nonetheless, both systems possess global octagonal symmetry as indicated by the diffraction patterns. The analysis of the tile orientations shows that in all three quasicrystal phases, tiles of the same shape occur in all possible orientations roughly with the same frequency, which is a common feature of random-tiling quasicrystals.[49]

All three quasicrystal configurations shown in Fig. 4 also contain local patches of periodic structures, such as square or hexagonal regions, which may compete with the quasicrystal phase in stability. However, we never observe long-term growth of these patches. Instead, over the course of the corresponding simulations, such patches are regularly formed and destroyed as defects or fluid regions diffuse through the system.

For a defect-free dodecagonal square-triangle quasicrystal, it is well-known that half of the total system area should occupied by squares, and the other half by triangles.[49,54] In other words, $\sigma = \tau = 1/2$, where σ is the area fraction occupied by squares, and τ is the area fraction occupied by triangles. Ignoring the defects that inevitably arise during our self-assembly process, the QC12 configuration shown in Fig. 4 corresponds to $\sigma = 0.491$ and $\tau = 0.509$. Given both the presence of defects and the periodic boundary conditions of our finite system, this is fully consistent with random quasicrystalline order.

For the QC8 phase, it is less obvious what tile concentrations we should expect in a perfect random quasicrystal. As illustrated in the center and right panels of Fig. 4, the relative concentrations of the different tiles we find in the self-assembled QC8 phase vary drastically as a function of the fraction of small spheres in the system. Since the S2 squares contain 4 small particles each, while the S1 squares only contain a single small sphere, higher compositions x_S favor a larger concentration of S2 squares. For high x_S, the QC8 tiling consists almost purely of large S2 squares and H1 triangles, with the triangles joined in pairs that form a thin rhombus. In this limit, the tiling can be seen as a mixture of just two types of tiles – square and rhombic – that are identical to the tiles that form *e.g.* the Ammann-Beenker[55,56] and Watanabe-Ito-Soma[57] octagonal aperiodic tilings. The same tiling – with different decorations of the tiles with particles – was previously observed in simulations of soft colloids,[33] particles with an oscillating interaction potential,[34,36] and patchy particles.[35] However, to our knowledge, no octagonal quasicrystals have yet been observed to

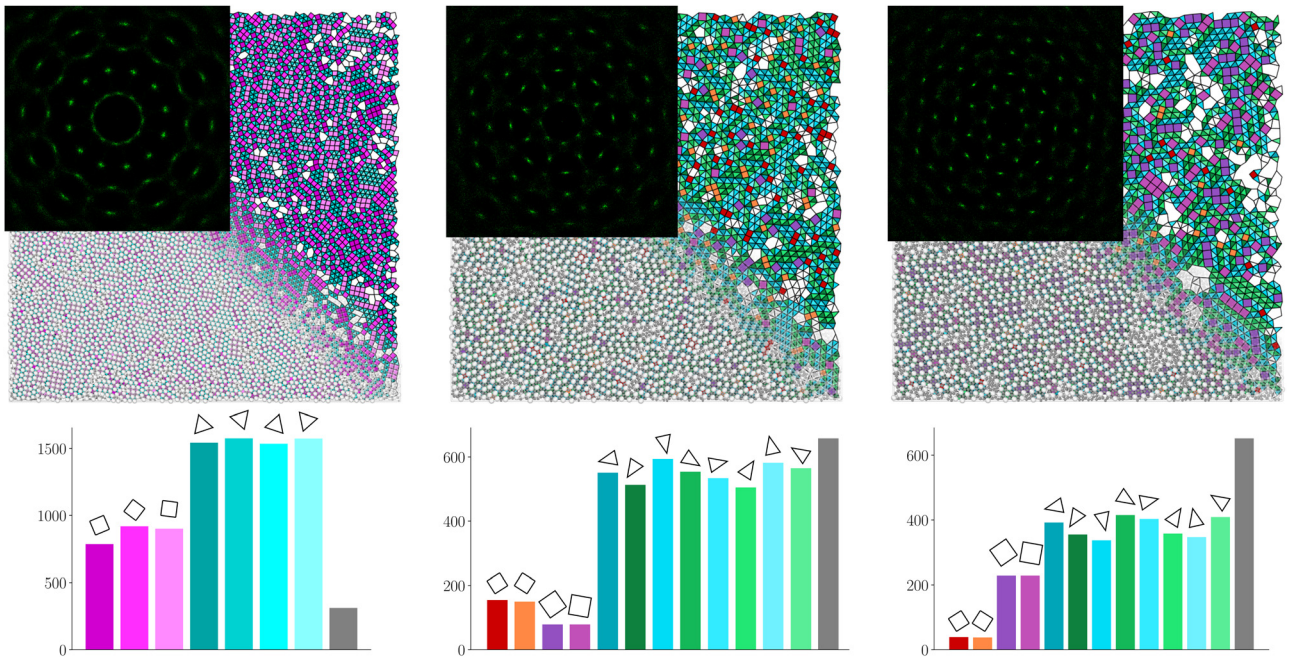

Fig. 4 Self-assembled dodecagonal and octagonal random-tiling quasicrystals in mixtures of 10^4 spheres on a flat plane, at state points (left QC12) $q = 0.45$, $x_S = 0.35$, $\eta = 0.84$, (middle QC8) $q = 0.5$, $x_S = 0.675$, $\eta = 0.86$ and (right QC8) $q = 0.55$, $x_S = 0.725$, $\eta = 0.84$. The underlying tilings are highlighted and tiles colored according to shape and orientation. The insets show the diffraction patterns, signaling the global 12 or 8-fold symmetries. Tile distributions (bottom) show the number of tile in each orientation in the tiling. The grey rightmost bar labeled denotes all defects.

spontaneously self-assemble in soft-matter experiments. In contrast, at low x_S the quasicrystal approaches a tiling of only H1 triangles and small S1 squares. Interestingly, a closely related tiling where the isosceles triangles are slightly deformed (breaking the 8-fold symmetry), was recently conjectured to be the densest-packed structure for a ternary mixture of hard disks.[58] Our findings suggest that a new QC8 quasicrystal made of these two tiles – isosceles triangles and small squares – should exist, along with a whole family of three-tile QC8 structures at different compositions. In this respect, our results exhibit completely new types of aperiodic octagonal tilings, which, to the best of our knowledge, have not yet been described in the literature.

It is interesting to consider under what conditions the QC8 tiling observed here can exhibit true 8-fold symmetry. Counting different orientations, this tiling consists of 12 different tiles: 2 orientations of large squares, 2 orientations of small squares, and 8 differently oriented isosceles triangles. In general, quasicrystal vertices can be seen as a projection of a high-dimensional lattice into a lower dimensional space.[54] As outlined in ref. 49, this representation can aid in determining the constraints on the relative concentrations of different tiles. As described in the ESI,† for a QC8 with octagonal symmetry we find the following constraint for the partial area fractions Σ, σ, and τ, associated with the large S2 squares, small S1 squares, and the triangles that make up H1, respectively:

$$\Sigma + (3 + 2\sqrt{2})\sigma - \tau = 0. \quad (4)$$

Additionally, since the entire area must be occupied by tiles, these area fractions must satisfy $\Sigma + \sigma + \tau = 1$. Since we know the composition of each tile in our binary mixture, it is straightforward to rewrite these constraints in terms of the fraction of small particles x_S, yielding:

$$\Sigma = \frac{2(4 + 3\sqrt{2})x_S - 4\sqrt{2} - 5}{6 - 4x_S} \quad (5)$$

$$\sigma = \frac{-(4 + \sqrt{2})x_S + 4}{6 - 4x_S} \quad (6)$$

$$\tau = \frac{-(8 + 5\sqrt{2})x_S + 4\sqrt{2} + 7}{6 - 4x_S} \quad (7)$$

In Fig. 5, we plot this prediction together with the measured tile concentrations in our self-assembled configurations of 10 000 particles. Note that in the analysis of the simulation data, we consider only the portion of the system covered by the three valid types of tiles and omit all defects. We find that the observed tile concentrations are essentially independent of size ratio and packing fractions within the investigated regime. Considering the fact that the analyzed configurations were the result of spontaneous self-assembly, and hence contain significant amounts of defects, the agreement is excellent, demonstrating that the system indeed favors tile compositions that correspond to an eight-fold quasicrystalline symmetry.

Finally, in order to quantitatively assess the quality of the quasiperiodic order, we measure the perpendicular strain (also often called phason strain[59] ‡) of the self-assembled structures. To this end, we associate each vertex in the tilings obtained at

‡ Note that there has been some debate in the literature with respect to the use of the word 'phason' when describing quasicrystal properties.[59,60]

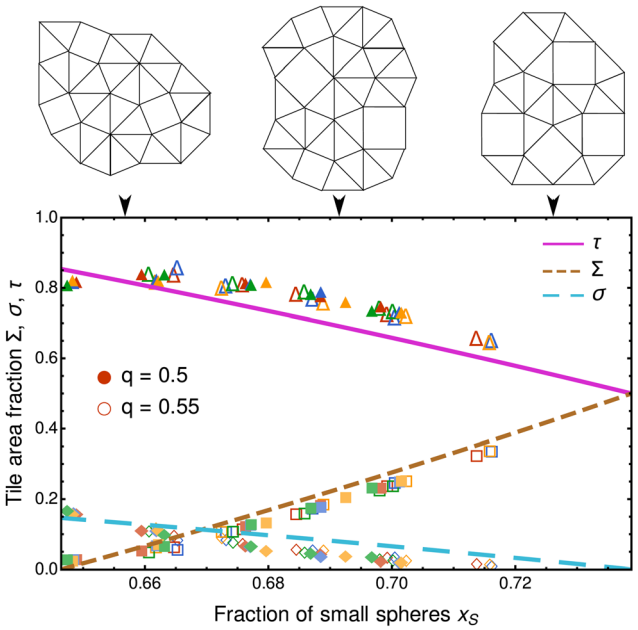

Fig. 5 Area fractions of the three different tiles in the QC8 tiling, Σ, σ, and τ, corresponding to the large squares, small squares, and triangles, respectively. The lines indicate the theoretical prediction on the assumption of a maximally symmetric and globally uniform eight-fold tiling with no defects. Points correspond to simulation results at size ratios $q = 0.5$ (full symbols) and $q = 0.55$ (open symbols). Different colors of points correspond to different packing fractions, with $0.855 \leq \eta \leq 0.87$ for $q = 0.5$ and $0.835 \leq \eta \leq 0.85$ for $q = 0.55$. For the simulation data, we only consider the area covered by non-defect tiles when calculating the composition x_S and the tile area fractions. At the top, three patches illustrate the evolution of the tilings with the composition. From left to right: primarily small squares, mixture of small and large squares and primarily large squares.

the end of the simulations to points in 4D spaces; a procedure known as lifting.[61,62] Dodecagonal and octagonal tilings are lifted to two different 4D spaces whose basis vectors are reported in the ESI.† This assigns to each particle a position in the 4D superlattice associated with the 2D quasicrystal. This position can then be projected either back to its 2D parallel-space position $\mathrm{r}_i^{\parallel}$ or its 2D perpendicular-space position $\mathrm{r}_i^{\perp}$. The parallel and perpendicular sub-spaces are orthogonal to each other, with the parallel subspace corresponding to the real space of our original quasicrystal lattice. The perpendicular strain is then measured from the relation between points separation in these two projections, following ref. 63. In particular, we examine the behavior of the perpendicular displacement $d^{\perp}$ as a function of $d^{\parallel}$, where for each pair of particles i and j, $d_{ij}^{\parallel/\perp} \doteq \|\mathrm{r}_i^{\parallel/\perp} - \mathrm{r}_j^{\parallel/\perp}\|$. For large distances in parallel space, the perpendicular displacement increases linearly with the separation in parallel space and its slope is a direct measure of the average perpendicular strain $\xi = \sqrt{\xi_1^2 + \xi_2^2}$ with $\xi_{1,2}$ the eigenvalues of the full 2×2 perpendicular strain matrix. For a quasicrystal with long range quasiperiodic order, the perpendicular strain is zero. Defective quasicrystals resulting from self-assembly however typically exhibit some residual perpendicular strain, while periodic phases have an intrinsic non-zero perpendicular strain. For all three configurations shown in Fig. 4, we show the behavior of the perpendicular displacement field in Fig. 6, and compare it to the perpendicular displacement of a reference periodic approximant structure (see ESI†). Clearly, the perpendicular strain in the self-assembled quasicrystals is non-zero, but significantly lower than that in the periodic approximants. In practice, we observe that the value of the measured average perpendicular strains depend significantly on the state point and fitting range, and is sensitive to the defects in our reconstructed tiling. Typically, our self-assembled structures contain long dislocation defects (see ESI†), which separate regions with significantly different perpendicular displacements. This may be the result of our self-assembly simulations taking place at relatively high pressures. Rather than forming *via* a single nucleation event, self-assembly of our quasicrystal phases tends to occur *via* the rapid formation of quasicrystal tiles throughout the simulation box, followed by a much slower relaxation that rearranges these tiles and allows different domains to coalesce.[64] This slow nature of this process means that it is difficult to obtain high-quality quasicrystals. We note that other simulation studies have found much lower perpendicular strain in quasicrystals,[63,65] but typically by considering clusters of quasicrystal in direct coexistence with a fluid, which likely allows for significantly faster relaxation.

6 Geometrical arguments for quasicrystal stability

The emergence of the QC12 phase in our system can clearly be understood from its stability in the infinite-pressure limit.

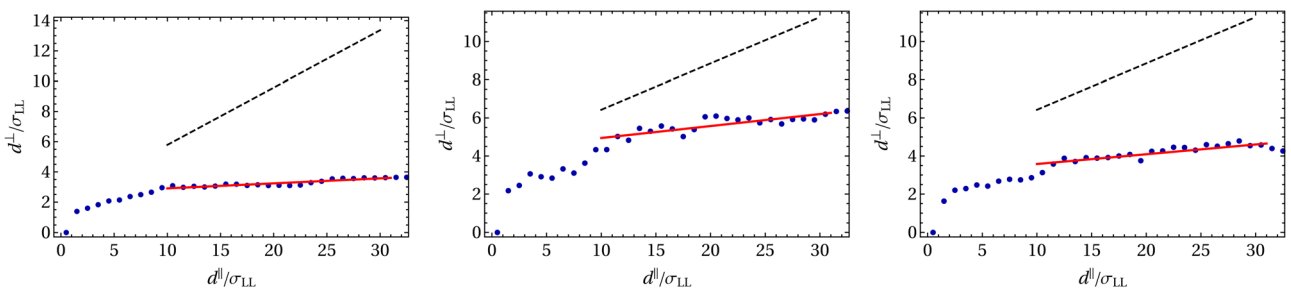

Fig. 6 The average perpendicular displacement $d^{\perp}$ as a function of the parallel-space displacement $d^{\parallel}$ for the three self-assembled quasicrystal configurations in Fig. 4. The red lines are linear fits to the large-distance behavior, with the slope related to the average perpendicular strain. For comparison, we also plot the corresponding line for a periodic approximant for each system (dotted black lines).

However, this is not the case for the QC8 phase: in the infinite-pressure limit, we find only periodic phases in the regime where QC8 was found to self-assemble. Hence, an intriguing question remains – is there a way to understand why these octagonal quasicrystals form? As stated, the three tiles that comprise the tiling are the small S1 square, the large S2 square, and the H1 triangle. In order to form the observed tilings, these shapes must have compatible edge lengths on their shared edges. In particular, the shared edges in the observed tilings are between the large square and the long edge of the H1 triangle, and the small square and the short edge of the H1 triangle. As shown in Fig. 7, the long edge of the triangle matches up almost exactly with the edge of a large square for size ratios between 0.5 and 0.6, in the region where we observe the self-assembly of this phase. Similarly, the short edge of the triangle and the small square match exactly for size ratios below $q = 2 - \sqrt{2} \simeq 0.59$. The fact that a QC8 with mainly small squares is not observed at size ratios below q = 0.45 can be understood from a packing argument. As shown in the inset of Fig. 7, when q is decreased below 1/2, the packing fraction of the triangle tile, which makes up the majority of the QC8 phase, decreases rapidly and drops below that of competing phases, such as the simple hexagonal lattice.

It is interesting to note that in the case of additive hard disks (or equivalently, spheres whose centers are constrained to a flat plane), we can still observe a regime where the three QC8 tiles match up geometrically, but in this regime their packing fraction is systematically lower than that of a hexagonal lattice (see ESI†). Consistently, in a self-assembly scan of additive hard disks in this regime we observed no quasicrystal self-assembly. Taken together, these observations suggest that the quasicrystal self-assembly requires both densely packed tiles and geometric edge-matching between them.

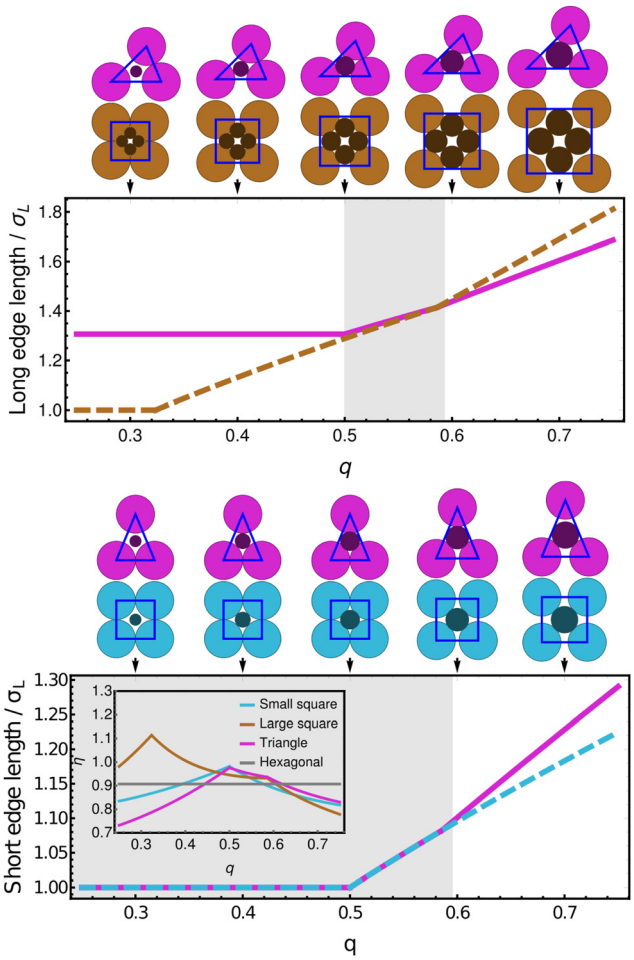

Fig. 7 Evolution of the possible long (top) and short (bottom) edge lengths as a function of size ratio. Matching regions are highlighted with a darker background. For size ratios between 0.5 and 0.6, long edges of the triangle and large square tiles on one hand, and short edges of triangle and small square tiles on the other hand match, thus allowing for the tiles that comprise the octagonal tiling to mix. The inset of the bottom graph displays the packing fraction of the three individual tiles, along with that of a coexistence of hexagonal packings of large and small particles. Self-assembly of QC8 is indeed observed for these values of the size ratio where edge lengths match and tiles pack better than Hex phases.

7 Discussion

In conclusion, we have explored the self-assembled phases that appear in binary mixtures of hard spheres on a flat plane. In addition to a variety of periodic crystals, we found that this very simple system is capable of forming two different quasicrystal structures: one dodecagonal, commonly observed in soft matter systems, and one octagonal which, to our knowledge, is described here for the first time. The octagonal quasicrystal consists of three distinct tiles, whose relative concentration can be continuously tuned by manipulating the number fraction of small spheres in the mixture, while maintaining the octagonal symmetry. Both observed quasicrystals self-assemble rapidly and reliably over a significant region of parameter space. The tiles proportions in the self-assembled octagonal quasicrystals are in remarkable agreement with theoretical predictions and their stability can be readily understood from geometrical arguments. We note that proving whether these quasicrystal phases are truly thermodynamically stable will require careful free-energy calculations, which we aim to explore in a future study.

In contrast to nearly all other numerical models that have been shown to form 2D quasicrystals, hard spheres on a flat plane can be realized experimentally on the colloidal scale, to the point of quantitative agreement between the experimental hard spheres and their ideal counterparts.[10,43] The simplicity of the model allows us to identify minimal ingredients for quasicrystal self-assembly: dense tiles with matching edges and entropy alone are sufficient to induce the formation of quasicrystals of different symmetries. Since many colloidal particles include a repulsive spherical core, these simple ingredients might explain quasicrystal formation in a broad range of soft matter systems, beyond hard-sphere colloids alone. This identifies hard spheres on a plane as a perfect candidate system for tackling fundamental open questions on quasicrystals, such as the dynamics of their nucleation, growth and annealing, the

role of their unique phason excitations or the dynamics of defects, both theoretically and in colloidal experiments on the micron scale.

Data availability

The data associated with Fig. 3, including all snapshots and scattering patterns, is available as a data package at: **https://doi.org/10.5281/zenodo.7712001**. To help view the data, HTML pages listing the results per size ratio are included.

Conflicts of interest

There are no conflicts to declare.

Acknowledgements

We thank Thomas Fernique, Jean-François Sadoc, Pavel Kalouguine, Alptuğ Ulugöl, and Anuradha Jagannathan for many useful discussions. EF, GF, and FS acknowledge funding from the Agence Nationale de la Recherche (ANR), grant ANR-18-CE09-0025. LF acknowledges funding from the Netherlands Organisation for Scientific Research (NWO) for a Vidi grant (Grant No. VI.VIDI.192.102). The authors acknowledge the use of the Ceres high-performance computer cluster at the Laboratoire de Physique des Solides to carry out the research reported in this article.

Notes and references

1 B. O'malley and I. Snook, *Phys. Rev. Lett.*, 2003, **90**, 085702.
2 U. Gasser, E. R. Weeks, A. Schofield, P. Pusey and D. Weitz, *Science*, 2001, **292**, 258–262.
3 B. De Nijs, S. Dussi, F. Smallenburg, J. D. Meeldijk, D. J. Groenendijk, L. Filion, A. Imhof, A. Van Blaaderen and M. Dijkstra, *Nat. Mater.*, 2015, **14**, 56–60.
4 D. Wang, T. Dasgupta, E. B. van der Wee, D. Zanaga, T. Altantzis, Y. Wu, G. M. Coli, C. B. Murray, S. Bals and M. Dijkstra, *et al.*, *Nat. Phys.*, 2021, **17**, 128–134.
5 A. Fortini and M. Dijkstra, *J. Phys.: Condens. Matter*, 2006, **18**, L371.
6 T. Curk, A. de Hoogh, F. J. Martinez-Veracoechea, E. Eiser, D. Frenkel, J. Dobnikar and M. E. Leunissen, *Phys. Rev. E: Stat., Nonlinear, Soft Matter Phys.*, 2012, **85**, 021502.
7 G. Jung and C. F. Petersen, *Phys. Rev. Res.*, 2020, **2**, 033207.
8 L. Fu, C. Bian, C. W. Shields, D. F. Cruz, G. P. López and P. Charbonneau, *Soft Matter*, 2017, **13**, 3296–3306.
9 F. Durán-Olivencia and M. Gordillo, *Phys. Rev. E: Stat., Nonlinear, Soft Matter Phys.*, 2009, **79**, 061111.
10 A. L. Thorneywork, J. L. Abbott, D. G. Aarts and R. P. Dullens, *Phys. Rev. Lett.*, 2017, **118**, 158001.
11 E. P. Bernard and W. Krauth, *Phys. Rev. Lett.*, 2011, **107**, 155704.
12 G. Foffi, W. Götze, F. Sciortino, P. Tartaglia and T. Voigtmann, *Phys. Rev. E: Stat., Nonlinear, Soft Matter Phys.*, 2004, **69**, 011505.
13 E. R. Weeks, J. C. Crocker, A. C. Levitt, A. Schofield and D. A. Weitz, *Science*, 2000, **287**, 627–631.
14 E. Zaccarelli, C. Valeriani, E. Sanz, W. Poon, M. Cates and P. Pusey, *Phys. Rev. Lett.*, 2009, **103**, 135704.
15 S. Marín-Aguilar, H. H. Wensink, G. Foffi and F. Smallenburg, *Phys. Rev. Lett.*, 2020, **124**, 208005.
16 E. Boattini, S. Marn-Aguilar, S. Mitra, G. Foffi, F. Smallenburg and L. Filion, *Nat. Commun.*, 2020, **11**, 1–9.
17 S. Pronk and D. Frenkel, *J. Phys. Chem. B*, 2001, **105**, 6722–6727.
18 B. van der Meer, F. Smallenburg, M. Dijkstra and L. Filion, *Soft Matter*, 2020, **16**, 4155–4161.
19 B. van der Meer, M. Dijkstra and L. Filion, *J. Chem. Phys.*, 2017, **146**, 244905.
20 P. N. Pusey and W. Van Megen, *Nature*, 1986, **320**, 340–342.
21 A. Yethiraj and A. van Blaaderen, *Nature*, 2003, **421**, 513–517.
22 R. P. Dullens, *Soft Matter*, 2006, **2**, 805–810.
23 C. P. Royall, W. C. Poon and E. R. Weeks, *Soft Matter*, 2013, **9**, 17–27.
24 T. Dotera, *Isr. J. Chem.*, 2011, **51**, 1197–1205.
25 D. V. Talapin, E. V. Shevchenko, M. I. Bodnarchuk, X. Ye, J. Chen and C. B. Murray, *Nature*, 2009, **461**, 964–967.
26 T. M. Gillard, S. Lee and F. S. Bates, *Proc. Natl. Acad. Sci. U. S. A.*, 2016, **113**, 5167–5172.
27 C. Duan, M. Zhao, Y. Qiang, L. Chen, W. Li, F. Qiu and A.-C. Shi, *Macromolecules*, 2018, **51**, 7713–7721.
28 F. Lançon, L. Billard and P. Chaudhari, *Europhys. Lett.*, 1986, **2**, 625.
29 M. Widom, K. J. Strandburg and R. H. Swendsen, *Phys. Rev. Lett.*, 1987, **58**, 706.
30 F. Lançon and L. Billard, *J. Phys.*, 1988, **49**, 249–256.
31 M. Widom, D. Deng and C. Henley, *Phys. Rev. Lett.*, 1989, **63**, 310.
32 M. N. van der Linden, J. P. Doye and A. A. Louis, *J. Chem. Phys.*, 2012, **136**, 054904.
33 M. Zu, P. Tan and N. Xu, *Nat. Commun.*, 2017, **8**, 1–9.
34 P. F. Damasceno, S. C. Glotzer and M. Engel, *J. Phys.: Condens. Matter*, 2017, **29**, 234005.
35 A. Gemeinhardt, M. Martinsons and M. Schmiedeberg, *EPL*, 2019, **126**, 38001.
36 G. Malescio and F. Sciortino, *J. Mol. Liq.*, 2021, 118209.
37 E. G. Noya, C. K. Wong, P. Llombart and J. P. K. Doye, *Nature*, 2021, **596**, 367–371.
38 P. K. Bommineni, N. R. Varela-Rosales, M. Klement and M. Engel, *Phys. Rev. Lett.*, 2019, **122**, 128005.
39 J. Wang, C. F. Mbah, T. Przybilla, B. Apeleo Zubiri, E. Spiecker, M. Engel and N. Vogel, *Nat. Commun.*, 2018, **9**, 1–10.
40 T. Dotera, T. Oshiro and P. Ziherl, *Nature*, 2014, **506**, 208–211.
41 H. Pattabhiraman, A. P. Gantapara and M. Dijkstra, *J. Chem. Phys.*, 2015, **143**, 164905.
42 X. Ye, J. Chen, M. E. Irrgang, M. Engel, A. Dong, S. C. Glotzer and C. B. Murray, *Nat. Mater.*, 2017, **16**, 214–219.
43 A. L. Thorneywork, R. Roth, D. G. Aarts and R. P. Dullens, *J. Chem. Phys.*, 2014, **140**, 161106.

44 E. Fayen, A. Jagannathan, G. Foffi and F. Smallenburg, *J. Chem. Phys.*, 2020, **152**, 204901.
45 C. Likos and C. Henley, *Philos. Mag. B*, 1993, **68**, 85–113.
46 L. Filion and M. Dijkstra, *Phys. Rev. E: Stat., Nonlinear, Soft Matter Phys.*, 2009, **79**, 046714.
47 G. Blind, *J. Reine Angew. Math.*, 1969, **1969**, 145–173.
48 M. Oxborrow and C. L. Henley, *Phys. Rev. B: Condens. Matter Mater. Phys.*, 1993, **48**, 6966.
49 M. Impéror-Clerc, A. Jagannathan, P. Kalugin and J.-F. Sadoc, *Soft Matter*, 2021, **17**, 9560–9575.
50 D. C. Rapaport and D. C. R. Rapaport, *The art of molecular dynamics simulation*, Cambridge University Press, 2004.
51 F. Smallenburg, *Eur. Phys. J. E: Soft Matter Biol. Phys.*, 2022, **45**, 22.
52 A. Haji-Akbari, M. Engel, A. S. Keys, X. Zheng, R. G. Petschek, P. Palffy-Muhoray and S. C. Glotzer, *Nature*, 2009, **462**, 773–777.
53 A. Haji-Akbari, M. Engel and S. C. Glotzer, *Phys. Rev. Lett.*, 2011, **107**, 215702.
54 D. Divincenzo and P. J. Steinhardt, *Quasicrystals: the State of the Art*, World scientific, 1991, vol. 11.
55 R. Ammann, B. Grünbaum and G. C. Shephard, *Discrete Comput. Geom.*, 1992, **8**, 1–25.
56 F. Beenker, *Algebraic theory of non-periodic tilings of the plane by two simple building blocks: a square and a rhombus*, Eindhoven University of Technology, 1982.
57 Y. Watanabe, M. Ito and T. Soma, *Acta Crystallogr., Sect. A: Found. Crystallogr.*, 1987, **43**, 133–134.
58 T. Fernique, A. Hashemi and O. Sizova, *Discrete Comput. Geom.*, 2021, **66**, 613–635.
59 M. de Boissieu, *Philos. Mag.*, 2006, **86**, 1115–1122.
60 C. Henley, M. De Boissieu and W. Steurer, *Philos. Mag.*, 2006, **86**, 1131–1151.
61 P. R. M. Baake and U. Grimm, *Aperiodic Order: A Mathematical Invitation*, Cambridge University Press, 2013, vol. 1.
62 M. Baake, D. Ecija and U. Grimm, *Z. Kristallogr. – Cryst. Mater.*, 2016, **231**, 507–515.
63 K. Je, S. Lee, E. G. Teich, M. Engel and S. C. Glotzer, *Proc. Natl. Acad. Sci. U. S. A.*, 2021, **118**, e2011799118.
64 W. Steurer, *Z. Anorg. Allg. Chem.*, 2011, **637**, 1943–1947.
65 M. Engel, P. F. Damasceno, C. L. Phillips and S. C. Glotzer, *Nat. Mater.*, 2015, **14**, 109–116.